

Supporting information for:

Contrasting motif preferences of platinum and gold nanoclusters between 55 and 309 atoms

Stephanie G. Lambie, Geoffrey R. Weal, Caroline E. Blackmore, Richard E. Palmer,
Anna L. Garden

1 Generating the ensemble of initial structures

Given the challenge associated with global optimisation of larger clusters, an ensemble of structures used to initiate the optimisations was generated that represents asymmetric clusters constructed from low-energy symmetric clusters of similar size.

It was found by some of us in an earlier publication[1] that only a relatively small energy penalty needs to be paid to create asymmetry on a cluster by removing atoms from either a (100) facet (FCC or Dh clusters) or from a corner (Dh clusters). The energy and structure of such a cluster can then be estimated as a linear interpolation between the parent closed shell cluster and that of the cluster formed when all atoms of a given type are removed. This principle was exploited in the current work whereby asymmetric clusters were formed by removing the requisite number of atoms from the (100) facets or corners of nearby closed shell clusters to yield an asymmetric cluster of the desired size. An example is given in Fig. 1. This process was also included for atoms from (111) facets to introduce more diverse starting guesses, even though the penalty for removing atoms from (111) facets is significantly higher.[1] For a cluster with a given number of atoms, there are many nearby closed-shell clusters that can be used to generate asymmetric clusters therefore many unique starting guesses are generated. For each constructed cluster, a local minimisation was performed.

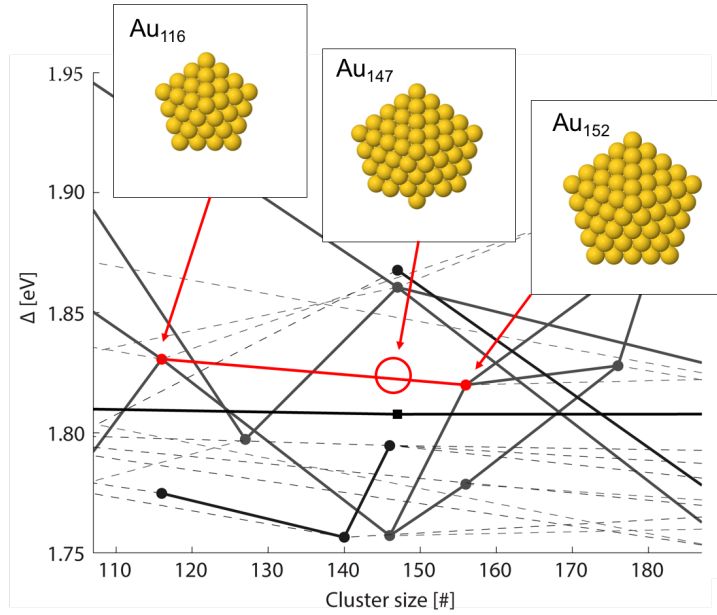


Figure 1: Example of generation of asymmetric clusters. Solid point indicate closed-shell clusters explicitly calculated using local minimisations and the RGL potential. Solid lines represent estimates of asymmetric clusters formed either by removing atoms from the (100) facets or corners (Dh only). Dashed lines represent estimates of asymmetric clusters formed either by removing atoms from the (111) facets. Red: Dh, Blue: FCC. The insets show the structures of the parent closed shell structures (Au_{116} and Au_{158}) as well as an asymmetric Au_{147} cluster formed by removal of 9 atoms from the (100) facet of the Au_{158} cluster.

2 Performance of the global optimisation

Ideally, a global optimisation (GO) algorithm would be able to locate the lowest energy structure from any given starting configuration. However, the potential energy surface of a cluster typically exhibits a set of characteristic funnels, in which each base motif creates a funnel in the potential energy surface, with very many minima within each funnel. For large clusters such as those in this study, the global optimisation procedure is very likely to get stuck in a funnel. A simulation initiated from, for instance, an Ih cluster is not very likely to transform to a Dh cluster over the course of the simulation. Furthermore, the very large number of minima within a given funnel means that even fully exploring a single funnel and locating the lowest energy structure of a given motif is a formidable task.

Table 1: The number of initial configurations and unique structures found from the global optimisation runs, for both Pt and Au in selected size brackets.

Cluster size	Au		Pt	
	Unique structures	Starting configurations	Unique structures	Starting configurations
54-56	11	46	13	55
99-103	62	90	67	90
224-232	121	162	150	162

These problems are illustrated in the present study where a large number of unique low energy structures were located from each of the GO runs beginning at different starting configurations, rather than converging on a single global minimum. Table 1 shows the number of unique structures found for each metal within the size brackets around 55, 101 and 228 atoms. Perfect performance of the global optimisation is obtained if only one unique structure (i.e. the global minimum) is found for each individual cluster size *i.e.* 3 unique structures for the 54-56 bracket (the global minimum at 54, 55 and 56 atoms), 9 unique structures for the 224-232 bracket and so on. The best performance was obtained for the smallest size bracket (54-56 atoms), for which 101 simulations yielded 24 unique structures across both Pt and Au. This indicates that while many of the simulations were able to explore the potential energy surface reasonably well, there were still many simulations that became “stuck” in local minima. For clusters that changed motif with respect to the starting structure, it was found that most of the structural changes were from FCC or Dh to the Ih motif.

As expected, as the size of the clusters increased, the GO performed worse and by the largest bracket the number of unique structures was very close to the number of starting guesses, suggesting that the optimisation algorithm was simply exploring a local region of the potential energy surface rather than more distant regions. This is expected for such large clusters, which was the motivation for initiating the algorithm from many different low-energy starting configurations.

3 Verification of global optimisation algorithm

To ensure that the results are not biased by either the choice of starting configurations or choice of GO algorithm, a number of alternative calculations were performed starting with randomly constructed initial configurations and using a different GO algorithm. A genetic algorithm (GA) was chosen as an alternative to the GOUST algorithm as it commonly used in cluster structure determination and, importantly, it explores the potential energy surface in a different way to GOUST. The GA was used to obtain the lowest energetic structures of Au and Pt clusters, of atom sizes 55, 56, 101 and 103. 55 and 101 were chosen as examples of systems for which a symmetric cluster exists that has complete facets and no adatoms (a closed-shell cluster). 56 and 103 atom clusters were chosen because no perfect cluster exists at these sizes and the lowest energy clusters have imperfect facets (open-shell clusters).

In the GA an initial population of 20 randomly constructed clusters was used; these clusters were locally minimised using the fast inertial relaxation engine (FIRE) local optimiser. A generation of 16 offspring was created (crossover rate = 0.8), where each offspring was created either by a crossover or mutation scheme and subsequently locally optimised. The mutation rate was set to 0.1. The crossover scheme used was the weighted cut and splice method[2, 3] while the mutation scheme used was to simply replace one of the clusters with another randomly generated cluster. The population was subjected to natural selection, where the offspring with lowest energies were retain at the expense of higher energy clusters. This process was repeated through multiple generations until all individuals in the population were of the same energy to two decimal places.

The energies of the lowest energy clusters obtained from each global optimisation algorithm for atom sizes 55, 56, 101 and 103 are shown in Table 2. It can be seen that, for all clusters considered, the cluster found by GOUST has an energy equal to or lower than that found by the GA. This test gives confidence that GOUST combined with the interpolation scheme for generating initial configurations does not bias the results obtained and in fact provides an advantage to obtaining reliable results. Furthermore, by initiating the GOUST calculations from clusters of different motifs we are able to explore more of the potential energy surface and identify low energy clusters of each motif, whereas the GA tended to explore only two of the three motifs.

Table 2: Energies of the most stable cluster obtained by the genetic algorithm (GA) and GOUST for the FCC, decahedral (Dh) and icosahedral (Ih) motifs as well the overall lowest energy structure. Bolded entries indicate the lower energy cluster; a “-” indicates that no cluster of a given motif was found.

Cluster	FCC [eV]		Dh [eV]		Ih [eV]		Overall [eV]	
	GA	GOUST	GA	GOUST	GA	GOUST	GA	GOUST
Au ₅₅	-195.25	-125.28	—	-195.21	-195.25	-195.25	-195.25	-195.28
Au ₅₆	—	-199.01	-198.88	-198.90	-198.88	-198.93	-198.88	-199.01
Au ₁₀₁	-363.95	-363.99	-364.06	-364.06	—	-363.79	-364.06	-364.06
Au ₁₀₃	-371.29	-371.46	-371.41	-371.41	—	-371.15	-371.41	-371.46
Pt ₅₅	—	-291.81	—	-291.88	-292.13	-292.13	-292.13	-292.13
Pt ₅₆	-297.31	-297.45	-297.47	-297.47	-297.12	-297.12	-297.47	-297.47
Pt ₁₀₁	-547.39	-547.36	-547.87	-547.87	—	-546.45	-547.87	-547.87
Pt ₁₀₃	-558.16	-558.67	-558.86	-558.86	—	-557.62	-558.86	-558.86

4 Motif dominance of Pt clusters soft-landed on carbon films

In Table 3 the motif dominance of synthesised Pt clusters between 10 and 600 atoms is shown. Over the whole range (10-600 atoms), there are roughly equal proportions of FCC and unidentified/amorphous (UI/A) clusters. When this range is broken into below and above 300 atoms it can be seen that, for the smaller clusters most clusters are UI/A whereas for the larger clusters, the FCC motif dominates.

Table 3: Percentage occurrence of each of the different motifs for the experimental Pt cluster generation over the whole size range (10-600 atoms), for all clusters less than 300 atoms and for all clusters greater than 300 atoms.

Size range	Motif			
	Dh	Ih	FCC	UI/A
10-600 atoms	2%	0%	43%	55%
<300 atoms	1%	0%	19%	80%
>300 atoms	3%	0%	66%	31%

5 Comparison of empirical potential and density functional theory

For clusters of more than 20 atoms, it is, in general, prohibitively expensive to perform a full global optimisation with DFT methods[4] and instead empirical potentials (EPs), such as the RGL potential used in this work, must be employed. However, it is common for EPs and DFT to disagree on the energetic ordering of clusters[5]. In this work, inaccuracy in the EP description may have two effects; namely that the EP may predict (i) the wrong ordering of the energies of clusters *within* a structural motif (e.g. the wrong FCC-based structures are predicted to be the most stable structure) and (ii) the wrong energy ordering *between* the Ih, Dh and FCC motifs. To address both of these issues, the three lowest energy structures from each motif as calculated by GOUST were retained and reoptimised with DFT.

Within a motif

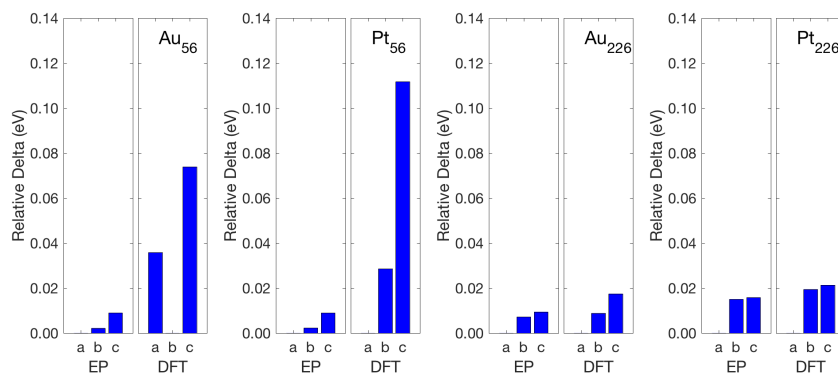


Figure 2: Relative stability of FCC clusters, calculated using EP and DFT. The three lowest energy FCC structures for each size from the GO algorithm (labelled a-c) are considered. Δ_{rel} gives an indication of stability relative to the lowest energy FCC cluster at that specific size, with either EP or DFT for each metal, where a lower Δ_{rel} indicates a more stable structure. Note that only the FCC motif is shown here, which does not necessarily reflect the lowest energy cluster in these size range.

The performance of EP and DFT for predicting the relative stability of clusters within a motif is shown in Fig. 2, using the FCC motif and clusters of 56 and 226 atoms as an example. When considering the relative ordering of the clusters, EP does not consistently agree with the DFT energy ordering of individuals within a given structural motif. For example, for Au₅₆, “FCC-a” is the lowest energy FCC cluster with the EP whereas DFT calculates “FCC-b” to be the most stable structure. This highlights the need to retain several low energy clusters of a given motif for optimisation using DFT, rather than simply taking the lowest energy structure as calculated by the EP. For the smaller clusters, the EP underestimates differences in stability between different structures of a given size. For larger clusters, the performance of EP and DFT is similar.

Between motifs

The performance of the EP and DFT treatments between motifs can be seen in Fig. 3, in which the motif with the lowest energy calculated using each approach is shown. Clearly, the agreement between EP and DFT is not consistent. For example, for Au, the Ih motif is never identified as being the lowest energy motif with EP, whereas it is the lowest energy motif on the DFT potential energy surface for several small clusters. There is no size range in which EP and DFT completely agree and, in fact, in some size brackets (e.g. Pt 224-232 atoms) there is complete disagreement between the two methods, clearly affirming the need to refine clusters obtained using EP with a higher level of theory to obtain a reliable estimate of cluster energetics.

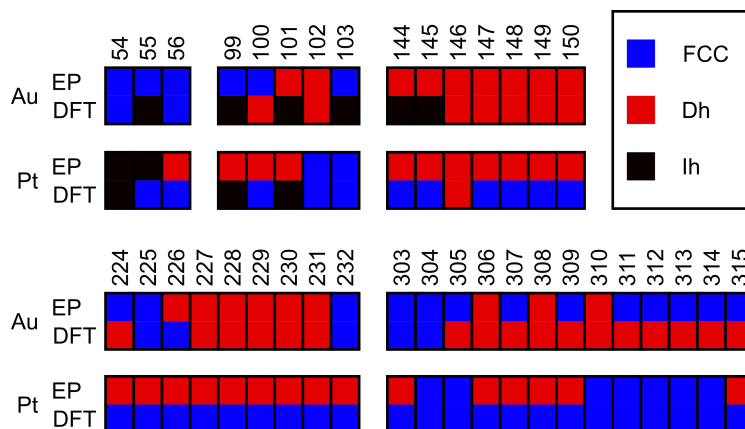


Figure 3: Structural motif of the lowest energy clusters for Au and Pt between 54 and 315 atoms, as calculated using an EP and DFT.

6 Quantity used to represent the stability of clusters

The stability of the lowest energy clusters in this study is represented in the main text in terms of the quantity Δ , which is defined as $\Delta = (E_{\text{tot}} - NE_{\text{bulk}})/N^{2/3}$, where E_{tot} is the energy of the cluster, N the number of atoms and E_{bulk} is the energy per atom in the bulk FCC crystal. Δ essentially divides the excess energy of the cluster by the approximate number of surface atoms, thereby enabling facile comparison of stability of clusters of different sizes. However, it has no effect on the relative stability of the different motifs, as can be seen in Figs. 4 and 5, where the stability mirrors that in Fig. 5 in the main text.

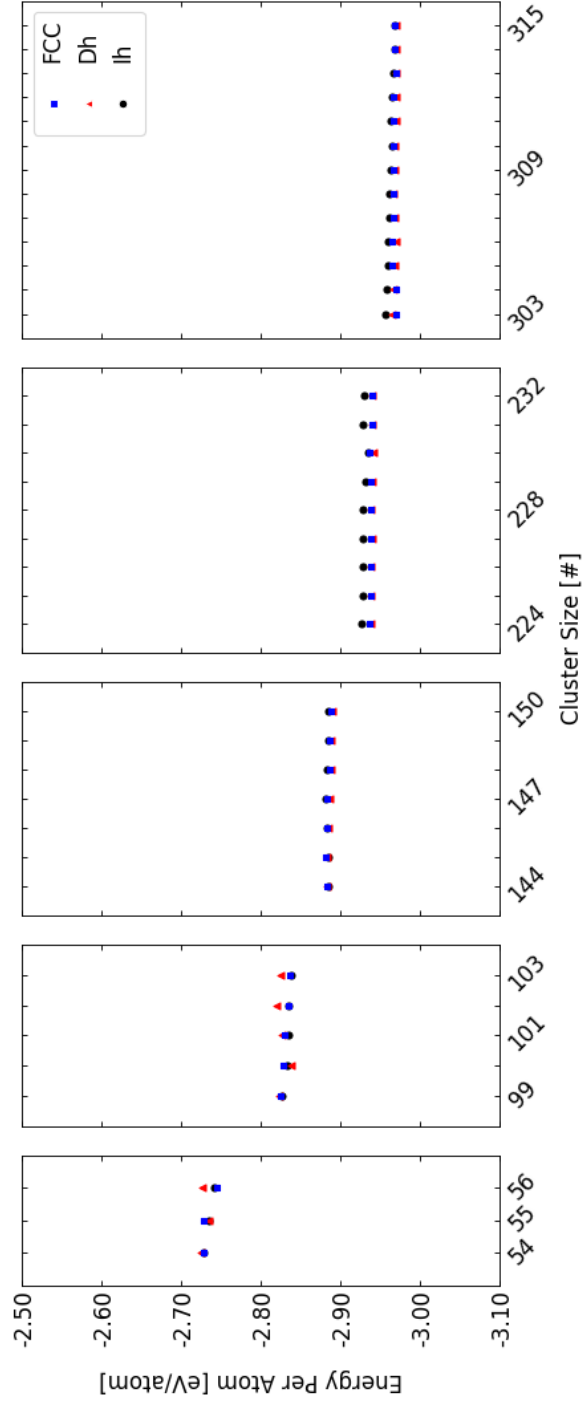


Figure 4: Lowest energy structures from each structural motif for Au clusters, as calculated using DFT; FCC (blue), Dh (red), and Ih (black). Stability of clusters is represented by energy per atom.

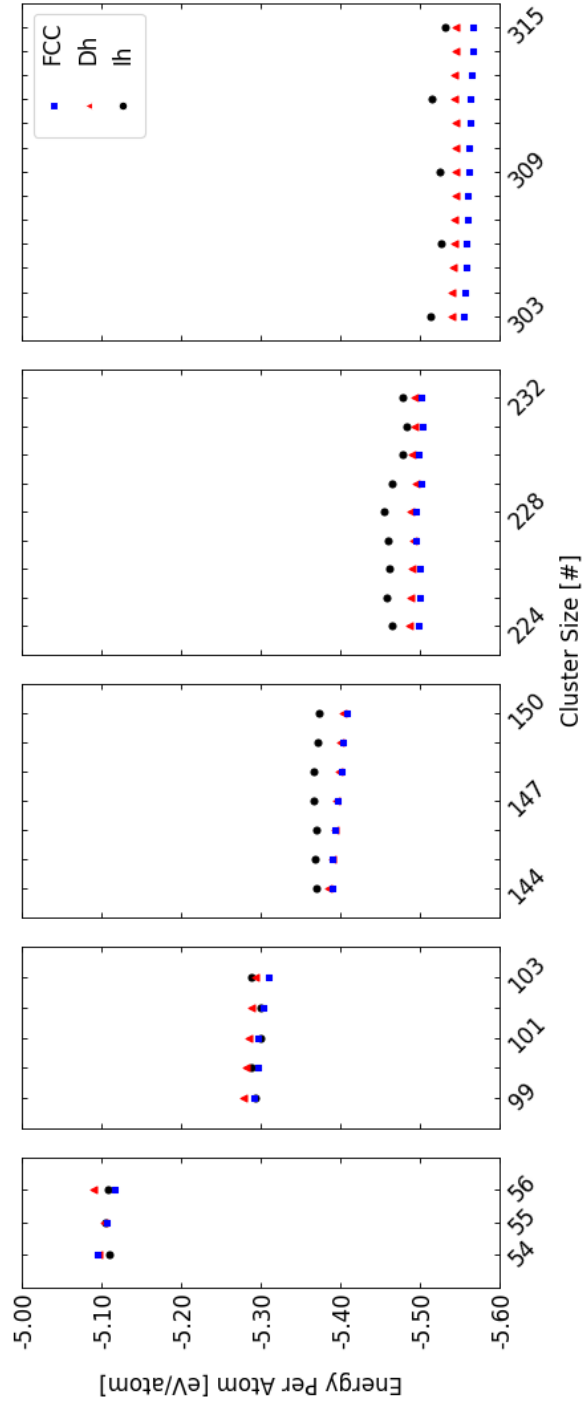


Figure 5: Lowest energy structures from each structural motif for Pt clusters, as calculated using DFT; FCC (blue), Dh (red), and Ih (black). Stability of clusters is represented by energy per atom.

7 Morphology of icosahedral clusters around 55 atoms

Several related Ih structures have been found for Au₅₅ in the literature and in this work. These structures are shown in Figs. 6, including the relative energies found using the EP and DFT approaches. The

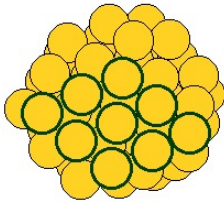
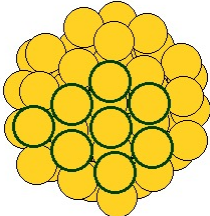
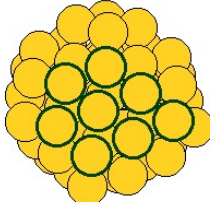
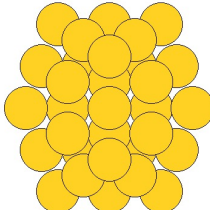
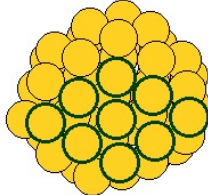
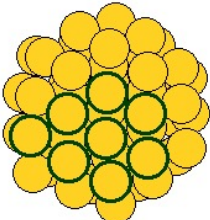
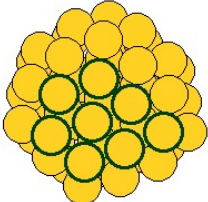
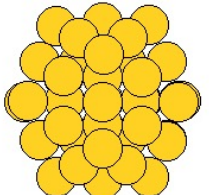
Au ₅₅ Ih Clusters				
Method	Garzón min.	EP min.	DFT min.	Perfect Ih
EP	 $E_{rel} = 0.003 \text{ eV}$	 $E_{rel} = 0.000 \text{ eV}$	 $E_{rel} = 0.020 \text{ eV}$	 $E_{rel} = 0.607 \text{ eV}$
DFT	 $E_{rel} = 0.175 \text{ eV}$	 $E_{rel} = 0.047 \text{ eV}$	 $E_{rel} = 0.000 \text{ eV}$	 $E_{rel} = 1.350 \text{ eV}$

Figure 6: Structures of four Au₅₅ clusters of interest, from left to right, the structure found by Garzón *et al.*, [6, 7, 8] the lowest energy Ih structure found using the EP, the lowest energy Ih structure found using DFT and the perfect Ih. On the Garzón structure, the characteristic rhombus shape is highlighted; on the EP and DFT minimum structures, a closely related feature is highlighted. The top and bottom rows show the same structures, but are normalized differently, dependent on the energetic ordering of the method being considered; EP (top) and DFT (bottom).

so-called Garzón structure is a chiral structure with a rhombus-shaped face, and has been identified as the global minimum in previous studies. [6, 7, 8] The EP and DFT minima are closely-related structures, with just one atom displaced. All three structures are rather close in energy on the DFT potential energy surface. For both the EP and DFT, the perfect Ih cluster is rather unstable.

Low energy Ih clusters for Pt₅₄ and Pt₅₅ are shown in Table 7. Using the EP approach, the perfect Ih (Pt₅₅) and Ih with a missing central atom (Pt₅₄) were found to be the lowest energy clusters. However, these structures were not the lowest energy on the DFT potential energy surface. With DFT, the minimum energy Pt₅₅ Ih cluster featured reconstructed “rosette” corners, also seen by Apra *et al.* for the same system. [9] A rosette corner is where six atoms form a ring with a central atom slightly depressed within the ring. In the present results one of the lowest energy Ih structures for Pt₅₄ cluster was found to have

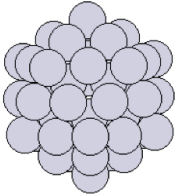
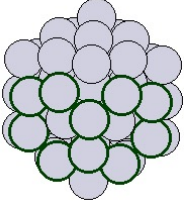
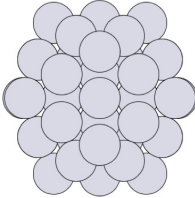
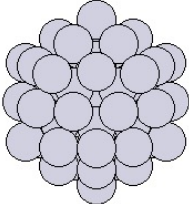
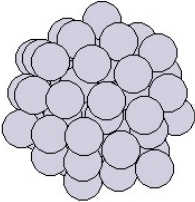
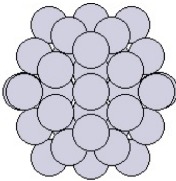
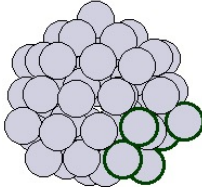
		Pt ₅₄ Ih Clusters		Pt ₅₅ Ih Clusters	
		Perfect [†] Ih	Double Rosette	Perfect Ih	
					
EP		$E_{rel} = 0.000$ eV	$E_{rel} = 0.581$ eV	$E_{rel} = 0.000$ eV	
		Perfect [†] Ih	Distorted Ih	Perfect Ih	Distorted Ih
					
DFT		$E_{rel} = 1.926$ eV	$E_{rel} = 0.000$ eV	$E_{rel} = 3.642$ eV	$E_{rel} = 0.000$ eV

Figure 7: Structures of Pt₅₄ Ih clusters of interest. The EP calculation finds the perfect Ih to be the lowest energy and the double rosette (highlighted on the structure) to be a low energy structure. DFT distorts the double rosette further, making this distorted structure the lowest energy Pt₅₄ Ih structure, while DFT finds the perfect Ih to be much higher in energy. [†]Denotes a perfect Ih missing the central atom.

a double rosette cluster (where two rosette features were adjoined on the surface of the cluster), when optimised using the EP. However, this same cluster rearranged upon relaxation with DFT refinement and the rosette features “softened” considerably. Nevertheless, in the DFT calculation of distorted clusters, some rosette-like features can still be observed.

8 Morphology of FCC Au clusters around 55 atoms

Morphology of the lowest energy FCC clusters, as calculated for Au using DFT, at 54, 55 and 56 atoms are shown in Figure 8. It is possible that the slight misalignment of the Au atoms in the FCC motif have hindered the appearance of parallel lines required for QSTEM identification of experimental clusters.

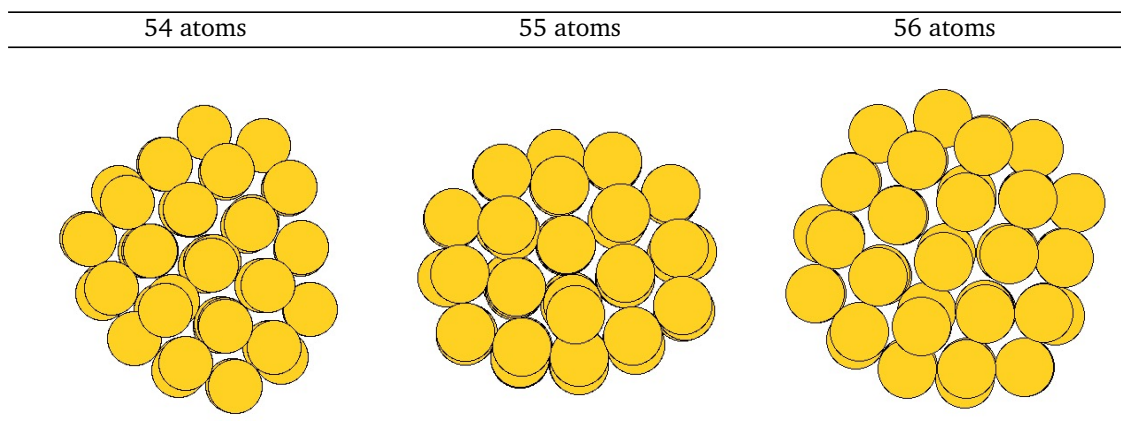


Figure 8: Structures of the lowest energy FCC clusters for Au in the 54- 56 atom size bracket. Note the slight misalignment of the atoms in each row could lead to the parallel lines in the QSTEM atlases being distorted.

9 Reassignment of experimental Pt clusters using new QSTEM atlases built on computational imperfect clusters

The lowest energy structures of some Pt clusters as found from the computational work here were used to reassign some of the experimental clusters that were initially assigned as unidentified or amorphous. This was achieved by generating QSTEM atlases of low energy clusters of each motif found using EP, which are typically somewhat distorted or asymmetric. The new QSTEM atlases for Pt₅₅ are shown in Figs. 9, 10 and 11. The clusters that were re-assigned using these new atlases are shown in Figs. 12, 13 and 14. The new QSTEM atlases for Pt₁₄₇ are shown in Figs. 15 and 16. The clusters that were re-assigned using these new atlases are shown in Figs. 17 and 18.

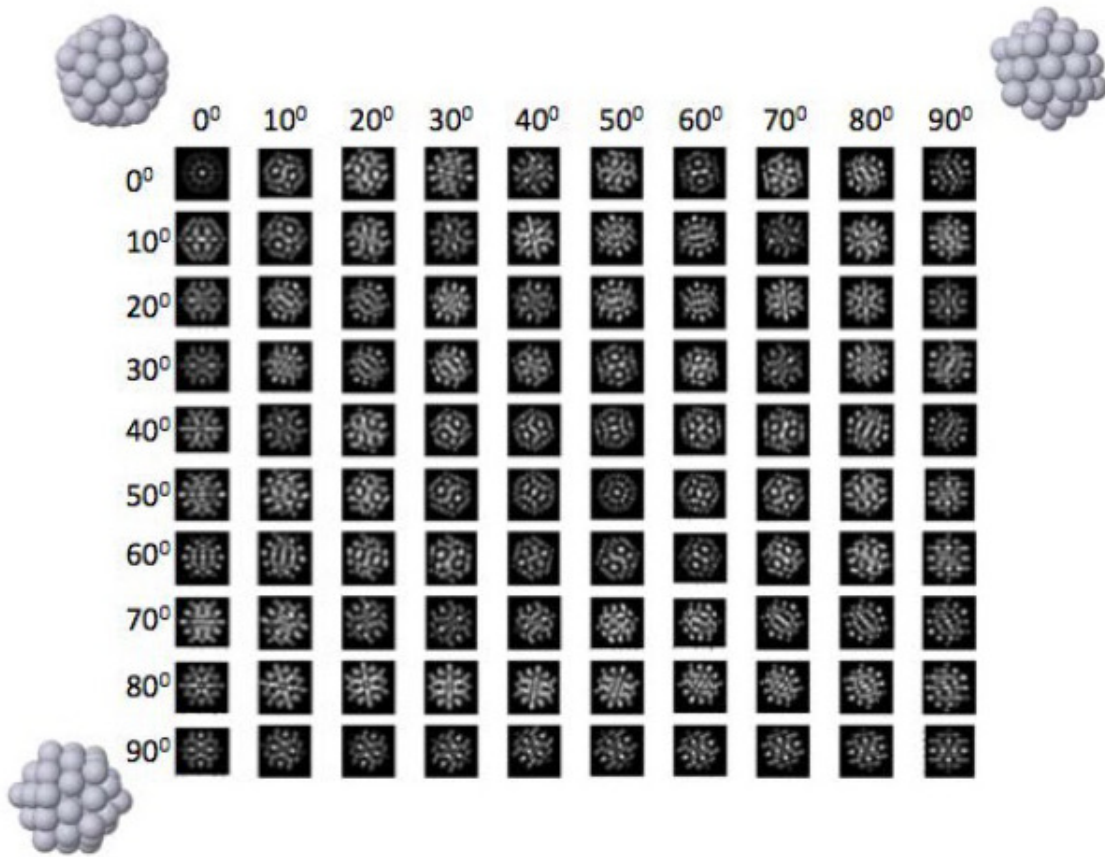


Figure 9: QSTEM simulation of the lowest energy Ih cluster for Pt₅₅. The clusters shown at the top left, top right and bottom left are the clusters for the 0°, 0°, the 90°, 0°, and the 0°, 90° projection, respectively.

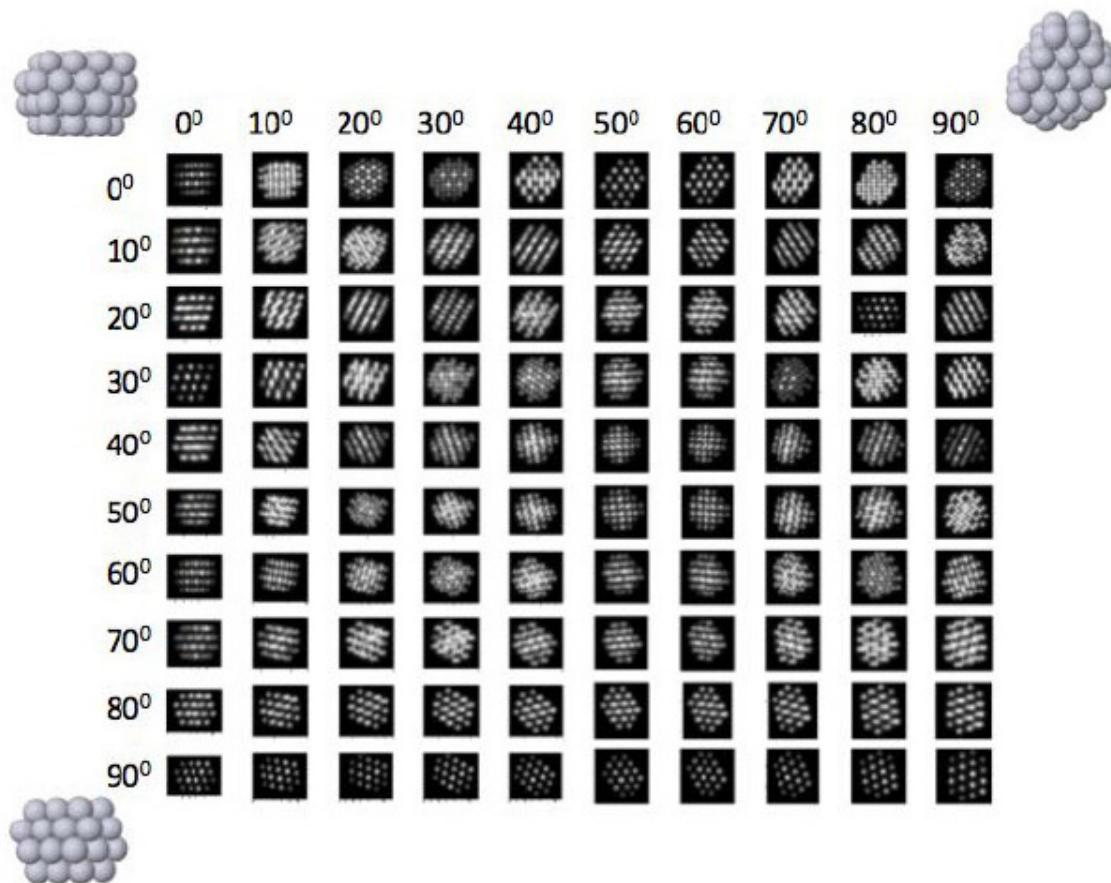


Figure 10: QSTEM simulation of the lowest energy FCC cluster for Pt₅₅. The clusters shown at the top left, top right and bottom left are the clusters for the 0°, 0°, the 90°, 0°, and the 0°, 90° projection, respectively.

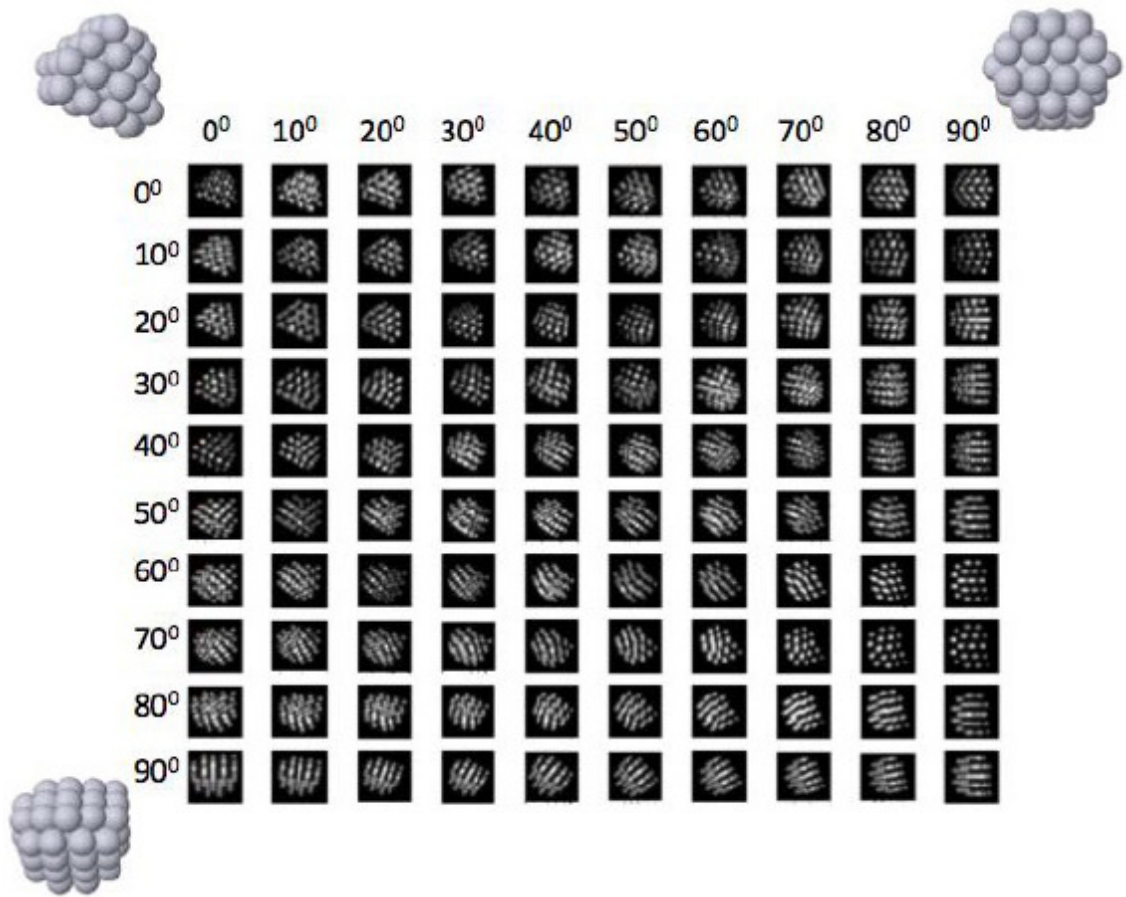


Figure 11: QSTEM simulation of the lowest energy Dh cluster for Pt₅₅. The clusters shown at the top left, top right and bottom left are the clusters for the 0°, 0°, the 90°, 0°, and the 0°, 90° projection, respectively.

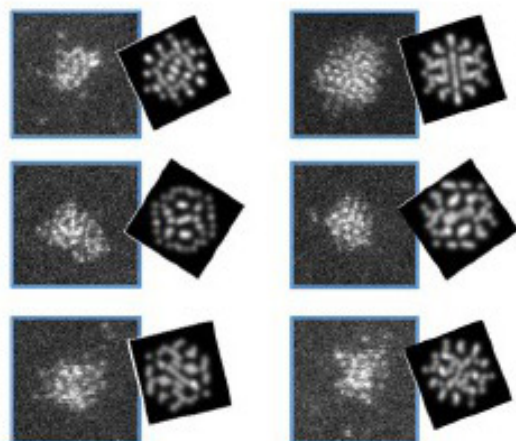


Figure 12: STEM images of 55 atom Pt clusters (blue edge) with matching new Ih QSTEM simulations. 6 of the 100 clusters were identified as Ih in motif.

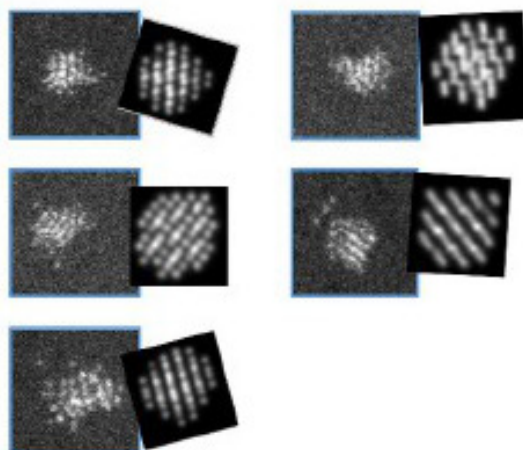


Figure 13: STEM images of 55 atom Pt clusters (blue edge) with matching new FCC QSTEM simulations. 5 of the 100 clusters were identified as FCC in motif.

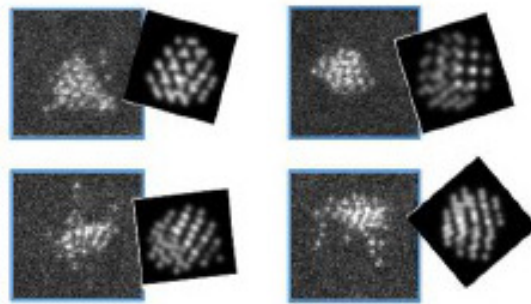


Figure 14: STEM images of 55 atom Pt clusters (blue edge) with matching new Dh QSTEM simulations. 4 of the 100 clusters were identified as Dh in motif.

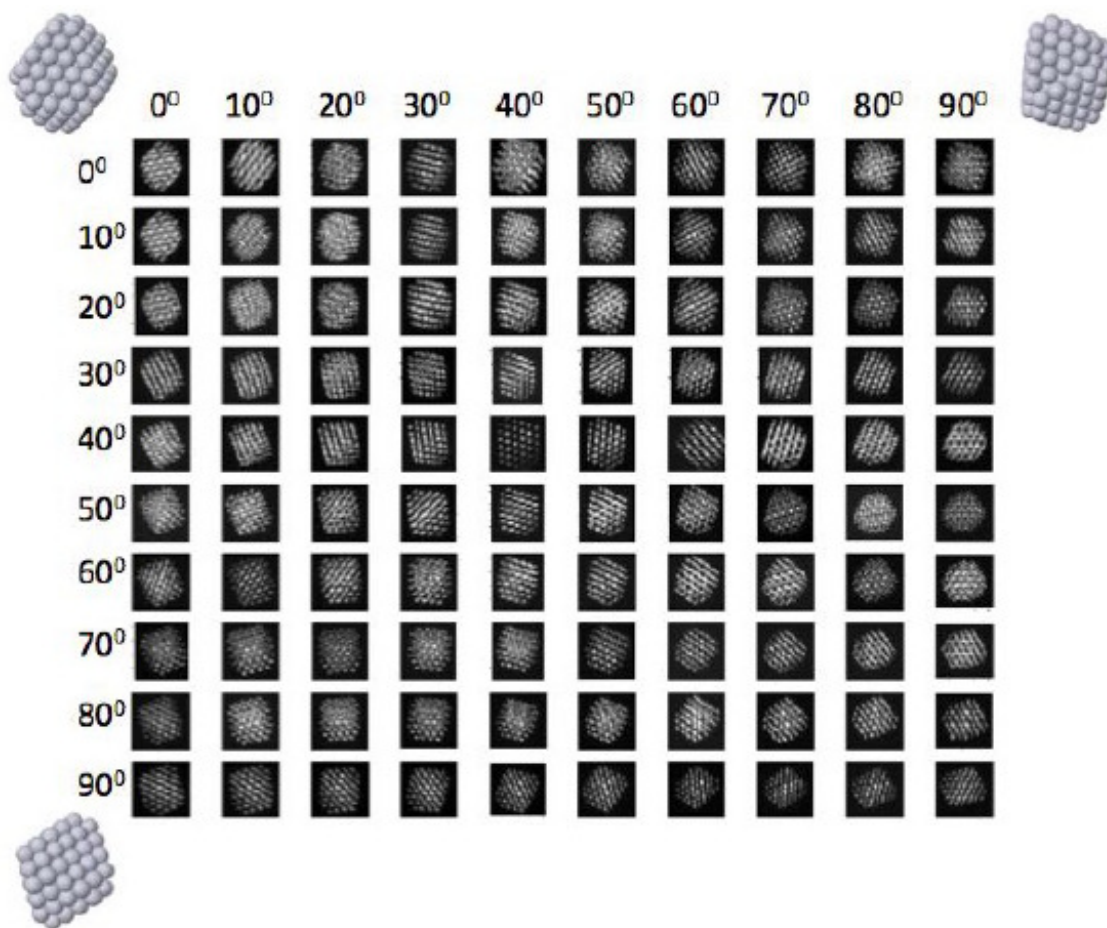


Figure 15: QSTEM simulation of the lowest energy FCC cluster for Pt₁₄₇. The clusters shown at the top left, top right and bottom left are the clusters for the 0°, 0°, the 90°, 0°, and the 0°, 90° projection, respectively.

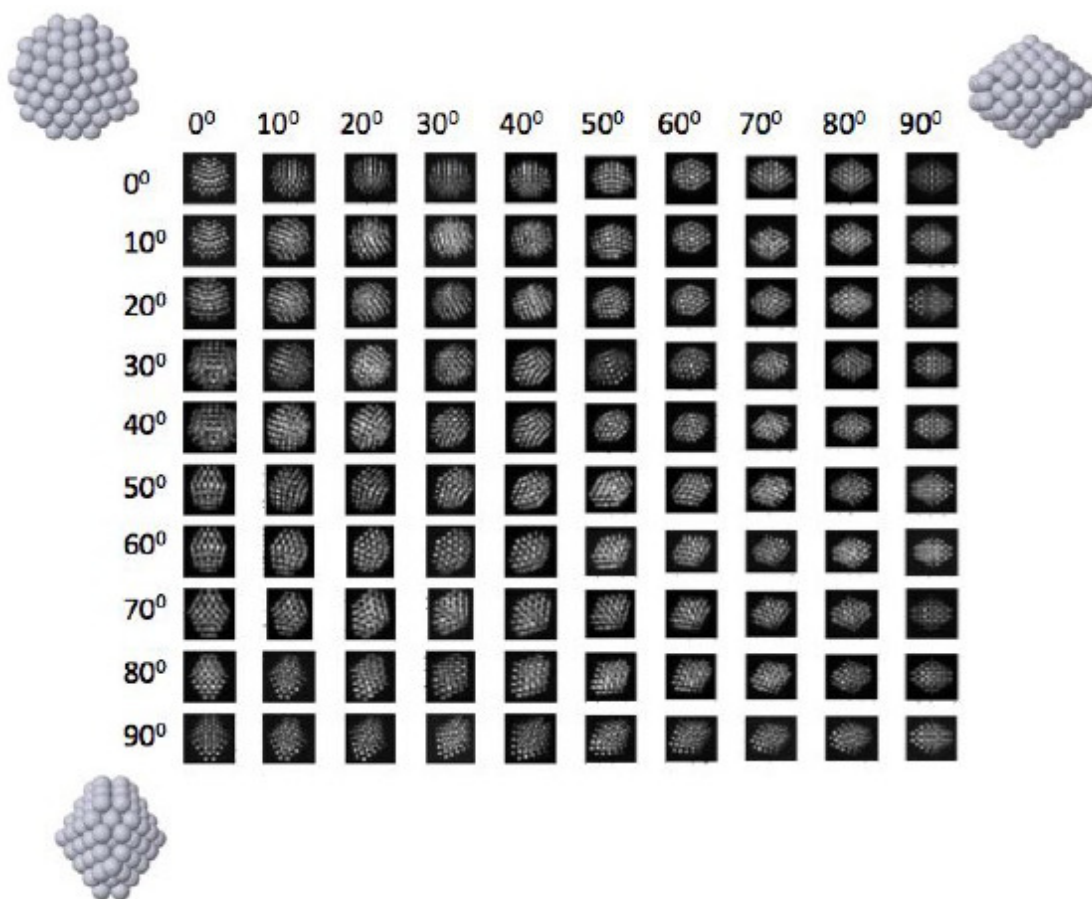


Figure 16: QSTEM simulation of the lowest energy Dh cluster for Pt_{147} . The clusters shown at the top left, top right and bottom left are the clusters for the $0^\circ, 0^\circ$, the $90^\circ, 0^\circ$, and the $0^\circ, 90^\circ$ projection, respectively.

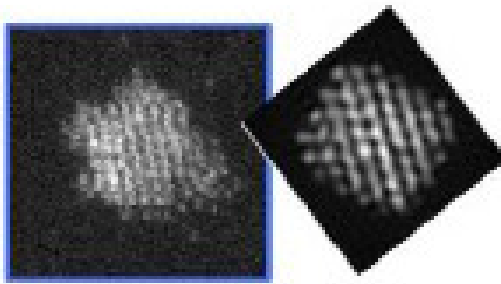


Figure 17: STEM images of 55 atom Pt clusters (blue edge) with matching new FCC QSTEM simulations. 1 of the 100 clusters were identified as FCC in motif.

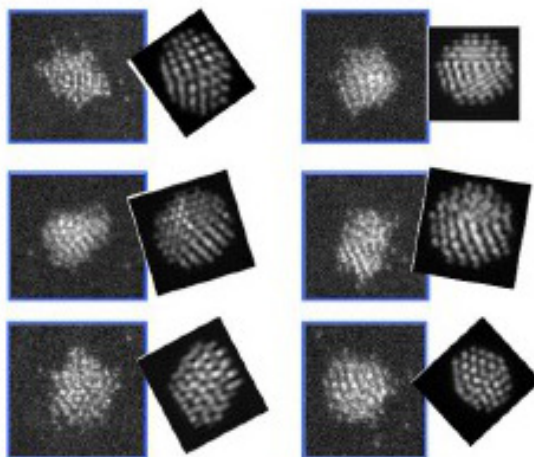


Figure 18: STEM images of 55 atom Pt clusters (blue edge) with matching new Dh QSTEM simulations. 6 of the 100 clusters were identified as Dh in motif.

10 Energies of closed shell Pt and Au clusters

The relative energies of selected closed shell clusters (Fig. 19) largely reflect the relative energies of the global minimum clusters (see Fig. 5, main text) but without the added complexity of the differences in structure. Therefore these structures are used to analyse the tendency towards amorphisation of Pt and Au clusters in the main text.

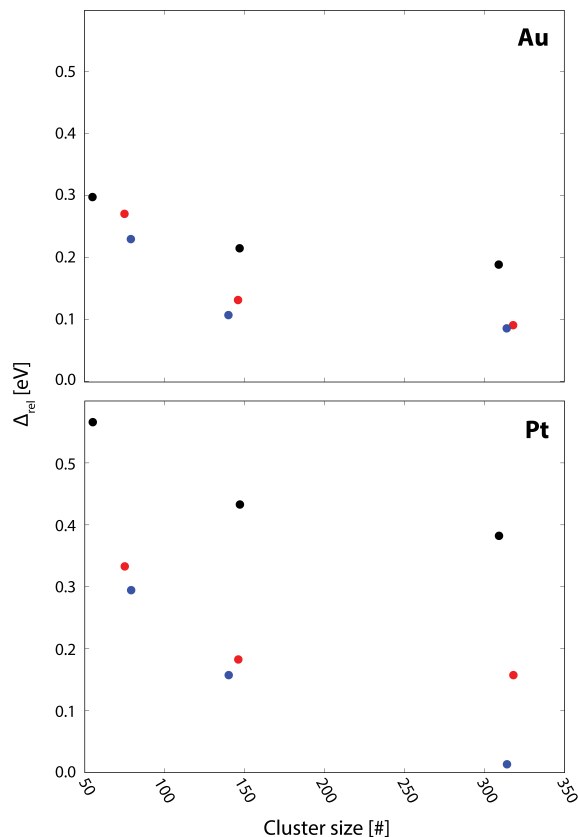


Figure 19: Relative stability of selected closed shell clusters calculated using DFT. Ih clusters (black) are the Mackay icosahedra with 55, 147 and 309 atoms. Dh clusters (red) are Marks decahedra with 75, 146 and 318 atoms. FCC clusters (blue) are truncated octahedra with 79, 140 and 314 atoms.

Some differences are in the energies of Au Ih clusters, which are slightly less stable for the closed shell clusters than the global minimum. The most notable difference, however, is for the Ih Pt₅₅ clusters. Considering the closed shell clusters, the Ih cluster is very unstable compared to the Dh and FCC motifs at this size. A significant lowering of the energy of this cluster is observed for the globally optimised structure ($\Delta\Delta = 0.25$ eV). As discussed in the main text, the lowest energy Ih clusters for Ih₅₅ clusters of both Au and Pt are highly disordered. This disorder leads to additional stability, which, for Pt is enough to make the Ih motif competitive.

References

- [1] Garden, A. L., Pedersen, A., Jónsson, H., “Reassignment of ‘magic numbers’ for au clusters of decahedral and fcc structural motifs,” *Nanoscale*, vol. 10, pp. 5124–5132, 2018.
- [2] D. M. Deaven and K. M. Ho, “Molecular geometry optimization with a genetic algorithm,” *Phys. Rev. Lett.*, vol. 75, pp. 288–291, 1995.
- [3] R. L. Johnston and C. Roberts, “Genetic algorithms for the geometry optimisation of clusters and nanoparticles,” in *Soft Computing Approaches in Chemistry*, vol. 120 of *Studies in Fuzziness and Soft Computing*, pp. 161–204, Berlin, Heidelberg: Springer-Verlag, 2003.
- [4] E. Aprà and R. Ferrando and A. Fortunelli, “Density-functional global optimization of gold nanoclusters,” *Phys. Rev. B*, vol. 73, p. 205414, 2006.
- [5] L. O. Paz-Borbón, R. L. Johnston, G. Barcaro, and A. Fortunelli, “Structural motifs, mixing, and segregation effects in 38-atom binary clusters,” *J. Chem. Phys.*, vol. 128, p. 134517, apr 2008.
- [6] Garzón, I. L., Reyes-Nava, J. A., Rodríguez-Hernández, J. I., Sigal, I., Beltrán, M. R., Michaelian, K., “Chirality in bare and passivated gold nanoclusters,” *Phys. Rev. B*, vol. 66, no. 7, p. 073403, 2002.
- [7] Garzón, I. L., Beltrán, M. R., González, G., Gutiérrez-González, I., Michaelian, K., Reyes-Nava, J. A., Rodríguez-Hernández, J. I., “Chirality, defects, and disorder in gold clusters,” *Eur. Phys. J. D*, vol. 24, no. 1, pp. 105–109, 2003.
- [8] López-Lozano, X., Pérez, L. A., Garzón, I. L., “Enantiospecific adsorption of chiral molecules on chiral gold clusters,” *Phys. Rev. Lett.*, vol. 97, p. 233401, 2006.
- [9] Aprà, E., Baletto, F., Ferrando, R., Fortunelli, A., “Amorphization mechanism of icosahedral metal nanoclusters,” *Phys. Rev. Lett.*, vol. 93, p. 065502, 2004.